Coupled wave packets study of the dynamics of dissociative ion–molecule charge exchange

F. Aguillon, V. Sidis, and J. P. Gauyacq

Citation: The Journal of Chemical Physics **95**, 1020 (1991); doi: 10.1063/1.461181
View online: http://dx.doi.org/10.1063/1.461181
View Table of Contents: http://scitation.aip.org/content/aip/journal/jcp/95/2?ver=pdfcov
Published by the AIP Publishing

Coupled wave packets study of the dynamics of dissociative ion–molecule charge exchange

F. Aguillon, V. Sidis, and J. P. Gauyacq
Laboratoire des Collisions Atomiques et Moléculaires (URA du CNRS No. 281), Université Paris-Sud, Bât 351, 91405 Orsay cedex, France

(Received 23 January 1991; accepted 8 April 1991)

A coupled wave packet method is presented which allows us to treat exactly the vibrational and dissociative motions in nonadiabatic atom–molecule collisions, whose relative motion is described by a classical trajectory. It consists of a time propagation of the coupled vibrational wave functions defined over a grid. It is applied to the dissociative charge exchange (DCE) process in atom–molecule collisions. Model cases are investigated that put forward the basic characteristics of the DCE process. Analysis of the time evolution of the wave packets leads to a direct view of the collision dynamics and to an interpretation of the dissociation mechanisms. Striking phenomena are revealed, that were not predictable by the previously existing approximate methods.

I. INTRODUCTION

Dissociative charge exchange (DCE) is a process defined by

$$A^+ + BC \rightarrow A + B^+ + C \qquad (1)$$

(or $A + BC^+ \rightarrow A^+ + B + C$). Such a process has been observed in a number of experimental situations, at collision energies ranging from less than 1 eV[1] to a few keV.[2] Existing theoretical treatments of DCE processes[3] made use of the semiclassical approximation, where the collisional A–BC motion is treated classically, while the electronic motion and the BC nuclear motion are treated quantum mechanically. Within this approximation, the charge exchange process is due to a time-dependent interaction between two rovibronic states of the BC molecule, the time dependence arising from the motion of the atom A along its classical trajectory.

In the semiclassical approximation, the usual way to treat such nonadiabatic processes is to expand the wave function describing the quantal degrees of freedom of the BC molecule on a rovibronic basis set,

$$\Psi = \sum_{j,v_j} a_{v_j}(t)\chi_{v_j}(\mathbf{r})\Phi_j(\boldsymbol{\rho};r,R,\gamma), \qquad (2)$$

where $\mathbf{r}$ is the BC vector, R is the A–BC distance, γ is the $(\mathbf{r},\mathbf{R})$ angle (Fig. 1), and $\boldsymbol{\rho}$ designates the coordinates of the electrons. Φ_j is a basis set of the electronic wave functions determined at fixed nuclei. It thereby depends parametrically on the nuclear coordinates R, r, and γ. χ_{v_j} is a rovibration wave function of the isolated molecule. One is thus led to solve a system of coupled differential equations involving the unknown a_{v_j} coefficients. Serious difficulties are met when the molecule dissociates during the collision or, more generally, when dissociative states are involved in the process. In such cases, there is an infinite number of basis wave functions χ_{v_j}, and then, an infinite number of coupled equations, which of course cannot be solved. In two particular situations, however, this problem can be overcome by resorting to relevant approximations, namely the sudden approximation and the local complex potential approximation.

The *rovibrational sudden approximation*[4] applies at *high collision energy*. It is based upon the slowness of the rovibrational motion of the BC nuclei compared to the relative A–BC motion. The BC molecule can be regarded as fixed in the laboratory frame during the whole collision. The DCE process reduces to an atom–atom-like charge exchange, exhibiting Stueckelberg interferences[5] due to multiple transitions between the bound and the repulsive state. After this charge exchange, the molecular ion BC^+ is left in a repulsive state, and dissociates. Since the transitions between the two electronic states are vertical transitions, the energy distribution of the dissociation products is governed by the reflection principle (Fig. 2).

At *low collision energy*, the sudden approximation breaks down, since the molecule may vibrate during the collision. However, for not too small collision energies, the molecular axis can be assumed to remain fixed in space during the encounter. Yet another approximation, namely the *local complex potential approximation* (LCP) now applies.[6] The LCP method is basically a perturbative approach; it considers the initial bound vibrational state of the BC molecule embedded in the dissociation continuum of BC^+ (Fig. 2).

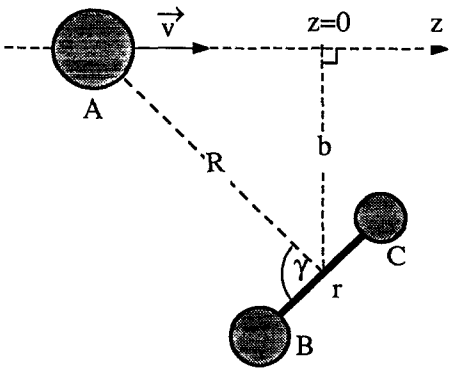

FIG. 1. Collision coordinates. The collision velocity v and the BC molecular axis are not necessarily in the same place.

 0021-9606/91/141020-13$03.00

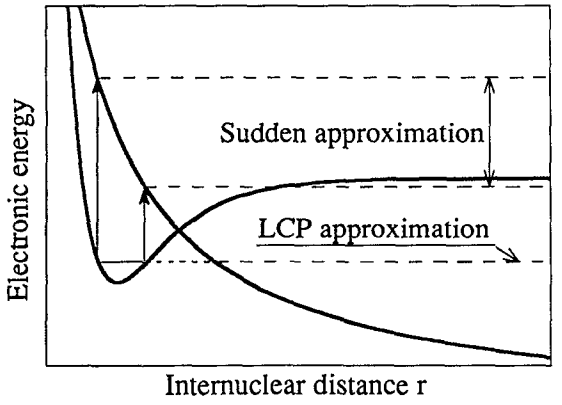

FIG. 2. Cuts along the r coordinate of typical diabatic energy surfaces governing the DCE process. When the collision energy is high, the transition between the bound initial state and the dissociative repulsive state takes place in a very short time; thus, DCE gives rise to a vertical transition from the bound to the repulsive state, followed by a dissociation on the repulsive energy surface. In such a case, the energy distribution is simply the shape of the initial probability density in the bound state "reflected" by the dissociative energy curve. On the contrary, when the collision energy is low and the coupling is weak, DCE can be regarded as the decay of the bound state embedded in the dissociation continuum. In that case, the dissociation energy distribution is peaked around the resonance energy.

Because of the coupling between the discrete and the continuum states, the discrete state is associated with a complex potential causing an irreversible decay of the bound state. Just as the Fermi golden rule, the LCP approximation is *valid when the interaction between the two states lasts long enough*. This restricts the range of validity of the LCP to collision times that are much longer than a vibrational period; moreover, as the LCP is a perturbative approximation, it is only valid for weak couplings. The LCP approximation leads to a dissociation energy spectrum peaked at the resonance energy, defined as that of the initial vibrational level relative to the asymptotic dissociative energy level (Fig. 2). Stueckelberg interferences do not show up; the dissociation probability increases monotonically when the coupling strength increases.

These two approximations have limited and disconnected ranges of applicability; they fail at intermediate collision energy (a few 10 eV) and/or in the strong coupling conditions. Moreover, they provide little insight into the dynamics of the process and the competition of DCE with elastic and inelastic scattering,

$$A^+ + BC \rightarrow A^+ + BC^{(*)} \tag{3}$$

as well as with collision induced dissociation (CID),

$$A^+ + BC \rightarrow A^+ + B + C. \tag{4}$$

The above methods were developed to eliminate the problem of an infinite set of coupled equations generated by the expansion (2). In order to be able to treat DCE in more general conditions, one has to forsake this expansion. The present work takes its inspiration from an earlier work[7] on electron detachment in a negative ion–atom collision

$$A^- + B \rightarrow A + B + e^-. \tag{5}$$

In that work, the difficulty of treating the bound–continuum transitions was removed by handling directly the time evolution of the electronic wave packet by using a completely numerical approach. This wave packet method has been widely used during the eighties (see, e.g., Ref. 8 and references therein). More recently, work has been reported on a curve crossing problem[9] and photofragmentation,[10] involving two-coupled wave packets. We shall use such a coupled wave packets method here to study the DCE process.

Expanding upon a previous brief account[11] about the wave packet study of DCE processes, the purpose of the present work is threefold:

- to design a unified treatment of DCE within the semiclassical approximation at any collision energy and coupling strength encompassing the domains of validity of the preexisting (vibrational sudden and LCP) approximations.

- to look for new effects in the domain that could not be treated by the preexisting approximations, especially the low energy/strong coupling case, where the most spectacular results should show up;

- to understand the dynamics of the DCE process.

The latter two objectives have led us to choose a very simple model case, from which all the nonessential features have been removed, in order to isolate the most prominent dynamical effects. Moreover, we have emphasized the study of typical cases: strong or weak coupling, high or low collision energy, to show the various characteristic behaviors of the wave packets, and then to discuss the dynamics of the DCE process.

II. DESCRIPTION OF THE METHOD

A. General equations

Instead of Eq. (2), the wave function of all the electrons and of the B and C nuclei is expanded according to

$$\Psi = \sum_j \mathscr{P}_j(\mathbf{r},t)\Phi_j(\boldsymbol{\rho};r,R,\gamma). \tag{6}$$

$\mathscr{P}_j(\mathbf{r},t)$ is the wave packet describing the BC nuclear motion: the instantaneous probability of finding the system with its $\mathbf{r}$ vector in a $d^3\mathbf{r}$ volume is simply $|\mathscr{P}_j(\mathbf{r})|^2 d^3\mathbf{r}$. In what follows, we shall restrict ourselves to two electronic states Φ_1 and Φ_2.

The Hamiltonian governing the system's evolution is split in two parts,

$$H = H_{el} + T, \tag{7}$$

where H_{el} is the electronic Hamiltonian of the ABC triatomic, while T is the rovibrational energy of the BC molecule. The electronic basis set Φ_j is chosen to be a diabatic basis set,[3,12] i.e., the kinetic energy of BC is not inducing any coupling,

$$\left\langle \Phi_j(\boldsymbol{\rho};r,R,\gamma) \left| \frac{\partial}{\partial q} \right| \Phi_k(\boldsymbol{\rho};r,R,\gamma) \right\rangle = 0, \tag{8}$$

where $q = r,R,\gamma$. Inserting Eq. (6) into the time-dependent Schrödinger equation leads to a set of coupled partial differential equations,

$$\left(i\hbar\frac{\partial}{\partial t} - T\right)\mathscr{P}_j(\mathbf{r},t) = \sum_k H_{jk}(r,R(t),\gamma(t))\,\mathscr{P}_k(\mathbf{r},t), \tag{9}$$

where

$$H_{jk}(r,R,\gamma) = \langle \Phi_j(\rho;r,R,\gamma)|H_{el}|\Phi_k(\rho;r,R,\gamma)\rangle_\rho. \quad (10)$$

At collision energies high enough (>1 eV), the collision takes place during a much shorter time than a rotational period of the BC molecule. The rotation can then be considered as frozen, and the wave packets, in this rotational sudden approximation, can be written as [4,13]

$$\mathscr{P}_j(\mathbf{r},t) = \frac{P_j(r,t)}{r}\mathscr{R}(\theta,\phi), \quad (11)$$

where θ and ϕ are the space fixed spherical coordinates of the r vector. $\mathscr{R}$ is independent of the time and of the electronic state j. It can then be factored out in Eq. (9), leading to

$$\left(i\hbar\frac{\partial}{\partial t} + \frac{\hbar^2}{2\mu}\frac{\partial^2}{\partial r^2}\right)P_j(r,t) = \sum_k H_{jk}(r,R(t),\gamma(t))P_k(r,t), \quad (12)$$

where μ is the reduced mass of the BC molecule.

In cases when the frozen rotation approximation breaks down, the rotation of the BC molecule could be treated directly by doing the calculation with a 3D wave packet: this would require a high amount of computation.

The set of coupled differential equations (12) is solved numerically, subject to the initial conditions,

$$\begin{cases} P_1(r,t_0) = G_{v_0}(r)\exp\left(\dfrac{-iE_{v_0}t_0}{\hbar}\right) \\ P_2(r,t_0) = 0 \end{cases}. \quad (13)$$

The subscript 1 refers to the electronic state correlated with $A^+ + BC$, and the subscript 2 denotes the electronic state correlated with $A + B^+ + C$. $G_{v_0}(r)$ is the vibrational wave function of the BC molecule in its initial state, and E_{v_0} is its energy.

Various pieces of information are easily extracted from the wave packets at the end of the collision ($t\to\infty$), e.g.,

-the survival probability in the initial vibronic state,

$$S_1(v_0) = |\langle G_{v_0}(r)|P_1(r,t\to\infty)\rangle|^2, \quad (14)$$

-the total survival probability in the initial electronic state,

$$S_1 = \langle P_1(r,t\to\infty)|P_1(r,t\to\infty)\rangle, \quad (15)$$

-the dissociation energy spectrum of the BC fragments,

$$\beta(e) = |\langle \chi_{2,e}(r)|P_2(r,t\to\infty)\rangle|^2, \quad (16)$$

where $\chi_{2,e}$ is the eigenstate of energy e for the electronic repulsive state, normalized to the energy scale. As will be seen below, the study of the probability densities $|P_1(r,t)|^2$ and $|P_2(r,t)|^2$ as functions of time provides physical insights into the dynamics of the collision.

The semiclassical approximation consists in treating the collision as a time dependent interaction $H_{12}(t)$ between two stationary states of the BC molecule. Thus, the above formalism can apply to any time dependent perturbation in a diatomic system (as long as the rotation can be regarded as frozen), e.g., vibrational excitation or photodissociation.

B. Prototype case

We have chosen to study as simple a prototype case as possible. It may seem rough and somewhat arbitrary, but its main purpose is to bring forward the dynamical characteristics of the DCE process and to ease the interpretations. Nonessential features, such as the R dependence of the diabatic potentials, have been left aside. It should be noted that the present simplifying assumptions are not essential to the method, and could be removed at will in studies of actual cases.

The BC molecule of our prototype case is chosen to have the same reduced mass μ and the same vibrational frequency ω as H_2. Moreover, the dissociative state of BC^+ has been built in such a way that it crosses the bound state near the minimum of its potential well. The relative disposition of the attractive and repulsive curves is such that the resonance energy is fixed to 3.25 eV. The diabatic potential energy hypersurfaces (Fig. 3) are assumed to depend exclusively on r, and have analytic expressions,

$$\begin{cases} H_{11} = \min[0.155(r-1)^2, 0.3] \text{ a.u.} \\ H_{22} = \min\{[1.52e^{-1.08(r+r_0)}(r+r_0)^{-0.813} \\ \qquad -0.110], 0.6\} \text{ a.u.} \end{cases} \quad (17)$$

The relative position of the curves is characterized by r_x, location of the crossing point. The parameter r_0 makes it possible to probe the influence of the relative position of the two energy curves, keeping the same asymptotic electronic energies. The two potentials were limited to absolute values smaller than 0.3 and 0.6 a.u., respectively. In order to limit the magnitude of the potential in Eq. (12), thereby allowing a better accuracy. The functional dependence of the H_{12} coupling, which is due to the considered charge exchange transition, is simply taken as [4,14]

$$H_{12} = H_{21} = 0.5e^{-R}f(\gamma)\text{a.u.} \quad (18)$$

On purpose, we let this interaction become quite large at small A–BC distances, to allow the probe of strong coupling

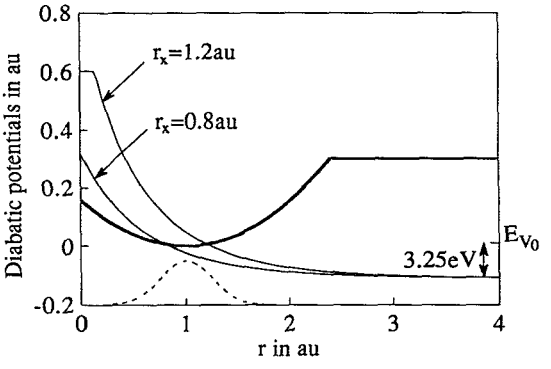

FIG. 3. Cuts of the diabatic potential energy surfaces in the present model. Since the surfaces are independent of both γ and R, only their r dependence is shown. The two dissociative potentials correspond to different relative positions of the bound (thick full line) and dissociative (thin full lines) states. The dashed line shows the probability density of the initial wave packet ($v=0$), whose energy relative to the dissociation asymptote is 3.25 eV.

cases at small distances of approach. Two angular dependences have been investigated,

-the isotropic case

$$f(\gamma) = 1 \tag{19}$$

corresponding to a spherical vibrator probes the R dependence alone,

-the so-called anisotropic case

$$f(\gamma) = \cos(\gamma) \tag{20}$$

corresponds to a DCE process involving an electronic transfer from an s atomic orbital to an antibonding orbital of the molecule whose electronic wave function vanishes between the two nuclei.

Finally, the straight line impact parameter approximation has been used,

$$R(t) = \sqrt{b^2 + v^2 t^2}\,, \tag{21}$$

where v is the collisional velocity and b the impact parameter. In this approximation, γ is simply given by

$$\cos[\gamma(t)] = \frac{b\sin(\theta)\cos(\phi) + vt\cos(\theta)}{R}, \tag{22}$$

where θ is the angle between the projection of $\mathbf{r}$ in the collision plane and the straight line trajectory, and ϕ is the angle between $\mathbf{r}$ and the collision plane. One can see that $\theta = \pi/2$ gives almost the same H_{12} functional dependence as that of the isotropic case. The anisotropic effects are related to the second part of the numerator in Eq. (22). They are expected to be the most important at $\theta = 0$; therefore, we have restricted ourselves to $\theta = 0$ to study the anisotropic case. The time evolution of H_{12} for the isotropic and anisotropic cases is displayed in Fig. 4. H_{12} is an even function of time in the isotropic case, and an odd function of time in the anisotropic case. Moreover, in the anisotropic case the coupling strength can exhibit a very fast time variation at small impact parameter.

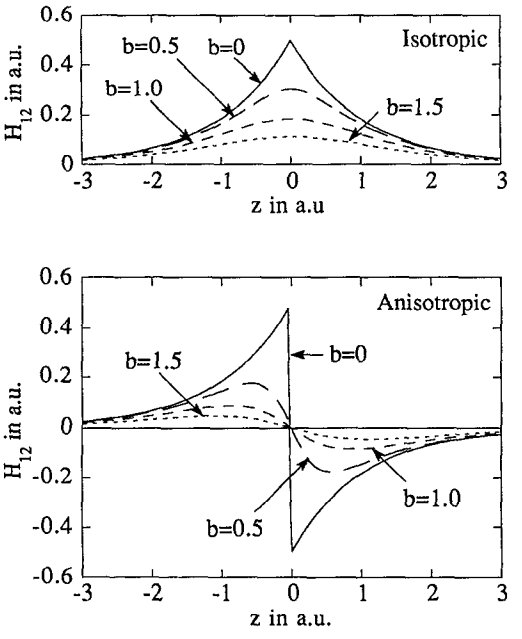

FIG. 4. Exchange interaction H_{12} in the isotropic case (upper frame) and anisotropic case (lower frame), as seen along the trajectory for different impact parameters.

C. Implementation

The set of coupled partial differential equations (12) is solved using a finite difference method. The wave packets are evaluated at the nodes of a two-dimensional grid defined by

$$\begin{cases} t_m = t_0 + m\delta t & 0 \leqslant m \leqslant N_t \\ r_n = n\delta r & 0 \leqslant n \leqslant N_r \end{cases}. \tag{23}$$

At each time step, the second order derivative $\partial^2/\partial r^2$ is evaluated using a five point formula

$$\frac{\partial^2 P(r_n,t)}{\partial r^2} = \frac{-P(r_{n-2},t) + 16P(r_{n-1},t) - 30P(r_n,t) + 16P(r_{n+1},t) - P(r_{n+2},t)}{12(\delta r)^2}. \tag{24}$$

The second-order difference scheme,[15]

$$P(r,t_{m+1}) = P(r,t_{m-1}) + 2\delta t\left(\frac{\partial P(r,t)}{\partial t}\right)_{t=t_m} \tag{25}$$

has been used to propagate in time in wave packets. The collision starts and stops at $R = 10$ a.u. The grid is initialized at the two first time steps,

$$P(r_n,t_m) = G_{v_0}(r_n)\exp\left(\frac{-iE_{v_0}t_m}{n}\right) \quad \begin{cases} 0 \leqslant n \leqslant N_r \\ m = 0,1 \end{cases}. \tag{26}$$

The first node of the spatial grid is always maintained to zero. This ensures the reflection condition and avoids numerical problems which would arise from the explicit introduction of an infinite repulsive potential at $r = 0$. It has been found that keeping the last spatial node to zero prevents propagation of numerical noise. The spatial grid is large enough to hold entirely the broadest wave packet. As the wave packets are of small extent at the beginning of the collision and much larger when the dissociation has occurred, the spatial size of the grid is gradually increased during the collision according to

$$N_r = N_{r_0}[1 + \alpha(t - t_0)]. \tag{27}$$

Care should be taken of the choice of δr and δt; otherwise stability problems may appear.[16] For the pure diffusive problem [i.e., Eq. (12) without right-hand side], with the 5-point finite difference formula (24) and the second order differencing time propagator (25), stability requires that the integration steps δr and δt verify,

$$\frac{\delta t}{(\delta r)^2} < \frac{3\mu}{8\hbar}. \tag{28}$$

In our case, the stability is actually achieved by taking $\delta t = 200\ (\delta r)^2$.

In order to ensure an accuracy of the dissociation probability better than 1%, the equations are first solved with $\delta t = 0.5$ a.u. and $\delta r = 0.05$ a.u.; they are then iteratively solved again with δt divided by $2^{2/3}$ and δr divided by $2^{1/3}$, as long as the dissociation probability as given by two successive computations differ by less than 0.01. Each iteration results in doubling the computation time. In extreme conditions (small collision velocity, small impact parameter), 2500 spatial steps and 29 000 time steps have been required.

III. RESULTS

A. Introduction

We have performed wave packets calculations in a wide range of conditions, determined by the isotropic or anisotropic behavior of the exchange interaction, and by the following parameters:

-the collision velocity v. The collisional time is obviously related to this parameter, and can be compared to the rotational and the vibrational periods of the BC molecule. The rotation of the molecule can be regarded as frozen if $v \gg 10^{-3}$ a.u. The collision time and the vibrational period are comparable when $v \simeq 0.03$ a.u. So-called low energy collisions correspond to $v < 0.03$ a.u. (the molecule may vibrate during the DCE process), and high energy collisions to $v \gg 0.03$ a.u. (the B and C nuclei do not move during the charge exchange process);

-the impact parameter b. In the straight line trajectory approximation, the coupling strength is only related to b. Strong coupling ($b < 2$ a.u.) and weak coupling ($b > 2$ a.u.) cases will be distinguished;

-the location r_x of the crossing point of the diabatic energy potentials H_{11} and H_{22}. Two values of r_x symmetrical with respect to the minimum of the H_{11} potential curve have been considered ($r_x = 0.8$ and 1.2 a.u.).

The initial vibrational state of the BC molecule has always been taken to be $v_0 = 0$.

Various types of results will be presented below: survival probabilities in the initial electronic state, energy spectra of the dissociation products, and time evolution of the probability density. In order to clearly illustrate the dynamics of the DCE process and to distinguish easily the various behaviors corresponding to the mentioned different conditions, the examples considered below are often obtained in extreme conditions: very weak or very strong coupling, very low or very high collision energy.

Although the calculation has always been performed in the diabatic basis set Φ_1, Φ_2, some of the interpretations will make use of the wave packets defined in the adiabatic basis set. The latter is obtained by diagonalizing H_{el} in the Φ_1, Φ_2 basis set. If the coupling between the diabatic states is much larger than their energy separation, the two adiabatic states are almost decoupled. The time evolution of the system is then easier to understand in the adiabatic basis.

B. Isotropic case

1. Basic behaviors of the wave packets

The simplest example of a time evolution of probability densities in the isotropic case is displayed in Fig. 5. Before entering into details about the dynamics of DCE, one can examine the kind of information that can be found in such a figure:

-firstly, the diabatic bound wave packet, associated with the electronic initial state, is prepared in the bell-shaped $v = 0$ state at the beginning of the collision ($t \ll 0$, or $z = vt \ll 0$). Unless collision induced dissociation [Eq. (4)] occurs, the wave packet remains near the bottom of the potential well ($r \simeq 1$ a.u.) during the entire collision. Oscilla-

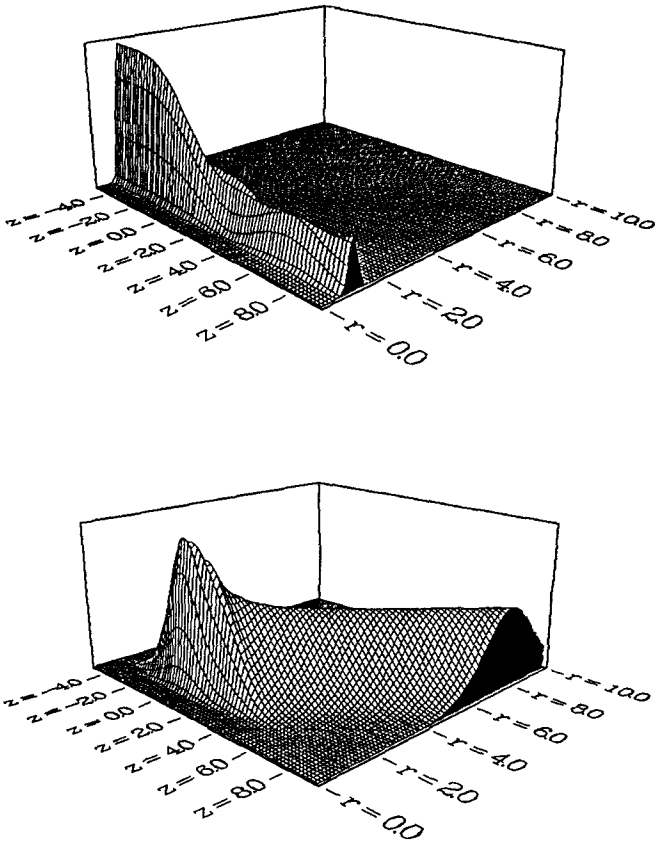

FIG. 5. Time evolution of the probability densities associated with the diabatic bound (upper) and dissociative (lower) states; r and $z = vt$ are as defined in Fig. 1. The probability densities are obtained in the following conditions: isotropic case, $b = 3.0$ a.u. (weak coupling), $v = 0.02$ a.u. (low collision energy), $r_x = 1.2$ a.u. At the beginning of the collision ($z = vt = -\infty$), the system is in the ground vibrational state of the electronic bound state. In the coupling zone, the probability density decreases in the bound state, while it grows in the dissociative state. At the end of the collision, the part of the initial wavepacket that has gone in the repulsive electronic state moves towards large r, thus describing dissociation. The part that survives in the bound state shows a small amount of vibrational excitation.

tion of the bound wave packet around its equilibrium position reveals vibrational excitation;

-secondly, the coupling between the electronic states induces a transition of the wave packet from the bound state to the dissociative state. When H_{12} is large, it can induce multiple transitions between the two states, leading to "vertical" oscillations of the wave packets;

-thirdly, the dissociation of the BC molecule means that $r \to \infty$, i.e., the dissociative wave packet moves to large r distances. Thus, a dissociation is seen in the repulsive state as a wave in the r, t plane (or r, z plane, since $z = v$);

-finally, strong interference structures will be observed when a wave packet is recombined after having followed at least two different paths.

Thus, the evolution of probability densities indicates when the transitions take place, if there are multiple transitions or multiple reaction channels, giving deep insight into the dynamics of the collision.

Figure 5 illustrates a DCE process in weak coupling conditions ($b = 3$ a.u.) and low collision energy (20 eV, i.e., $v = 0.02$ a.u.). It is easily seen that the initial bound wave packet is simply decaying in the vicinity of the turning point. Concurrently, the wave packet in the repulsive state grows. As time evolves, this wave packet moves outward thereby describing dissociation. This kind of DCE was readily understood within the LCP approximation.[6] Though both methods give essentially the same results, the wave packet method shows evidence for some vibrational excitation in the bound state [Eq. (3)].

The second example that is presented (Fig. 6) is very different: both the collision velocity ($v = 0.1$ a.u.) and the coupling strength ($b = 0$) are large. As the collision evolves in time, multiple transitions occur between the attractive and the repulsive electronic states. Owing to the considered high velocity, these transitions take place at a fixed position of the BC nuclei. The dissociation only occurs after the charge exchange. This case clearly belongs to the domain of validity of the sudden approximation.[4] As the B and C nuclei do not move, each slice of the molecular wave packet corresponding to a given r behaves exactly as in an atom–atom process, and exhibits the well known Stueckelberg interference pattern.[5] Both the above probability density for the dissociative state versus t at $b = 0$ and the dissociation energy spectrum versus b (Fig. 7) display an oscillatory pattern. Although they correspond to different objects, their shapes are comparable, exhibiting in particular the same number and amplitude of oscillations. These oscillatory patterns actually have the same origin. Indeed, the transitions of the wave packet between the electronic states are faster when the coupling increases, i.e., when b decreases. At $b = 0$, the number of oscillations is roughly 3.2. When b increases, the coupling decreases, and the number of oscillations of the wave packet decreases. Each time the number of oscillations is an integer, there is no dissociation. Thus, there is the same number of oscillations in the evolution of the dissociative wave packet for $b = 0$ and in the energy spectrum versus b, b varying from zero to infinity.

In Figs. 5 and 6, one clearly identifies two different motions: firstly, a wave packet in the electronic state tends to dissociate; secondly, transitions between the two electronic states due to the exchange interaction give rise to oscillations of the wave packets. The first two examples presented above were chosen such as only one of the two motions is present:

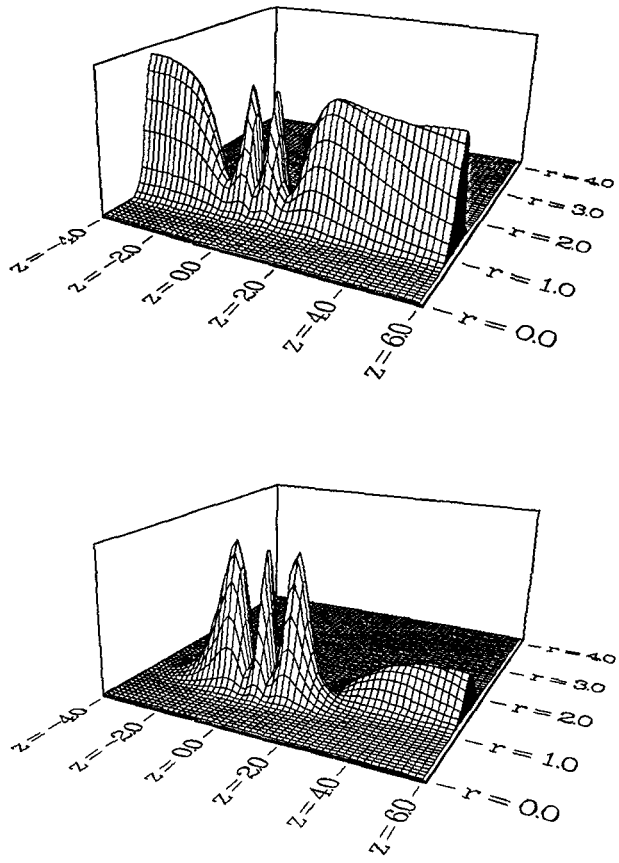

FIG. 6. Same as Fig. 5, except for $b = 0$ a.u. (strong coupling) and $v = 0.1$ a.u. (high collision energy). The wave packet, initially prepared in the ground vibrational state, oscillates between the two electronic states in the strong coupling region. The oscillations stop, i.e., the charge transfer process is over, before the wave packets can significantly move.

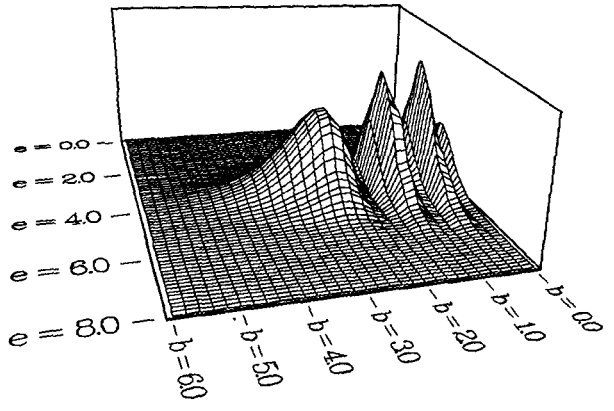

FIG. 7. Energy spectrum of the dissociation products as a function of impact parameter b, in the isotropic case, for $v = 0.1$ a.u. (high collision energy) at $r_x = 1.2$ a.u. The dissociation energy e is in eV, and the impact parameter b is in a.u. The structure seen as a function of b is a Stueckelberg interference pattern.

On Fig. 5, the system dissociates without oscillating between the two electronic states, whereas on Fig. 6, the system oscillates a few times without dissociating during the collision. In the following, the wave packet method will allow us to handle the interplay of the two motions.

2. General behavior of the wave packets

To foresee the behavior of the wave packets in the general case, one can notice that the two motions are somewhat mutually exclusive. Indeed, the oscillation between the two electronic states mainly concerns the part of the wave packets where $|H_{11}(r) - H_{22}(r)| < H_{12}(R)$, while the dissociation drives the wave packet into a region where $|H_{11}(r) - H_{22}(r)|$ is large. Conversely, when the coupling is strong, the wave packet can be considered to spend half of the time on an attractive potential, and half of the time on a repulsive one, thus inhibiting the dissociation motion. As a consequence, DCE mainly occurs in the intermediate coupling zone. This can be seen on Fig. 8(a), illustrating a DCE process at low energy and strong coupling: the dissociative wave packet is emitted before and after the turning point, i.e., in the regions where the exchange interaction is not too large. In the vicinity of the turning point [Fig. 8(b)], the "dissociative" wave packet does not dissociate significantly. However, its behavior is somewhat more complicated than one could have expected: it exhibits damped oscillations. This damping phenomenon can be understood using the adiabatic basis set.

The adiabatic wave packets P_1' and P_2' are defined by

$$\begin{pmatrix} P_1'(r,t) \\ P_2'(r,t) \end{pmatrix} = \begin{pmatrix} \cos[\alpha(r,t)] & -\sin[\alpha(r,t)] \\ \sin[\alpha(r,t)] & \cos[\alpha(r,t)] \end{pmatrix} \begin{pmatrix} P_1(r,t) \\ P_2(r,t) \end{pmatrix}, \tag{29}$$

where α is given by

$$\tan[\alpha(r,t)] = \frac{2H_{12}(t)}{[H_{11}(r) - H_{22}(r)] + \sqrt{[H_{11}(r) - H_{22}(r)]^2 + 4H_{12}^2(t)}}. \tag{30}$$

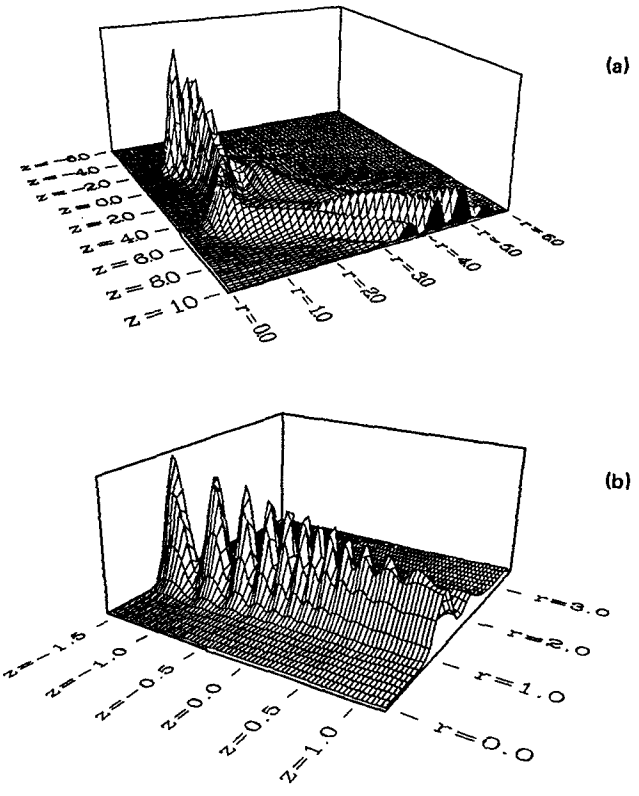

FIG. 8. Time evolution of the probability densities associated with the dissociative diabatic state in the isotropic state, for $b = 0$ a.u. (strong coupling), $v = 0.02$ a.u. (low collision energy), and $r_x = 0.8$ a.u. The lower part of the figure shows an expanded view of the $z \approx 0$ region. Most of the features governing DCE in the isotropic case can be observed here. Firstly, the wave packet can escape only in the intermediate coupling zone ($z \simeq \pm 3$), and it does not move in the strong coupling zone. Secondly, the dissociation is not complete in the first half of the collision, although a strong interaction has been applied during a long period of time. Thirdly, the part of the wave packet emitted at $z < 0$ is slower than the part emitted at $z > 0$; the latter one catches the former one up, giving rise to spatial interference effects. This slowing down effect is easily interpreted in the adiabatic basis set (see the text).

In the strong coupling region, the diabatic dissociative wave packets as a function of the adiabatic wave packets are given by

$$P_{1,2}(r,t) \simeq \frac{\sqrt{2}}{2} [P_2'(r,t) \pm P_1'(r,t)]. \tag{31}$$

When the adiabatic basis is the "good" basis, the two adiabatic wave packets are uncoupled. The different phases developed by the two wave packets give rise to interferences in the time structure of the diabatic wave packets in the r region where both P_1' and P_2' amplitudes are significant. In the case of Fig. 8(b), P_1' and P_2' are localized in the same r region when entering the strong coupling zone. Although P_2' does not escape towards large r, it slightly moves. As soon as P_2' starts moving, the r region where P_1' and P_2' significantly overlap narrows; this results in the damping of the $P_{1,2}$ oscillations. Thus, oscillations of the diabatic wave packets occur only at the beginning of the collision, and are damped as soon as the dissociation begins [Fig. 8(b)].

An interpretation of the dissociation probability as a function of b for various r_x values (Fig. 9) can also be found using the adiabatic basis set. For $r_x = 1.2$, the dissociation probability reaches 1 in the strong coupling region, whereas for $r_x = 0.8$, it saturates around 0.5, being accompanied by a significant vibrational excitation of the target. Indeed, the P_1 wave packet, initially prepared in the diabatic bound state, splits into two parts: P_2' which follows the lowest adiabatic energy curve, and P_1' which follows the upper adiabatic en-

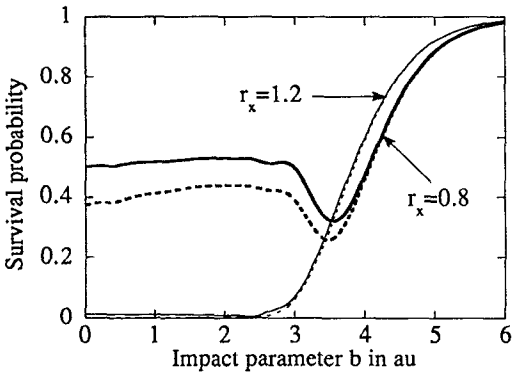

FIG. 9. Survival probability in the initial electronic state (full lines) as a function of the impact parameter b, obtained in the isotropic case, with $v = 0.02$ a.u. (low collision energy). The dashed line represents the contribution of the ground vibrational level. Two sets of results are presented ($r_x = 0.8$ and 1.2 a.u.). In the strong coupling region ($b < 3$ a.u.), the survival probability is very sensitive to the relative position of the diabatic energy curves.

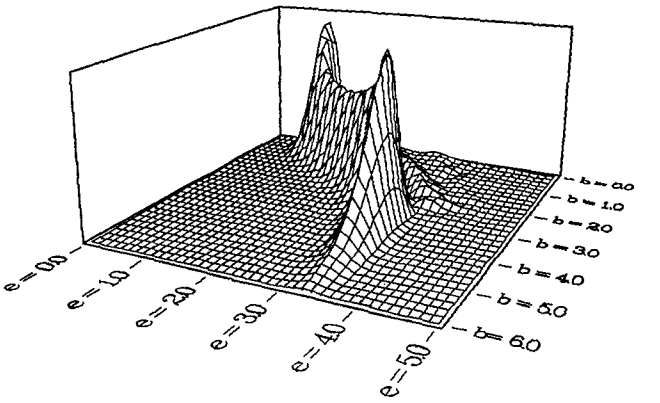

FIG. 11. Same as Fig. 7, except for $v = 0.02$ a.u. (low collision energy). In the weak coupling region ($b > 3$ a.u.), the energy distribution is centered on the resonance energy ($e = 3.25$ eV). In the strong coupling region, the dissociation products are much slower.

ergy curve. The P_1' wave packet is preserved against dissociation, as long as the adiabatic basis set remains a "good" basis set. The initial wave packet lies mainly in the adiabatic upper state when $r_x < 1$ (Fig. 10). Accordingly, the survival probability is expected to be smaller for $r_x > 1$ than for $r_x < 1$.

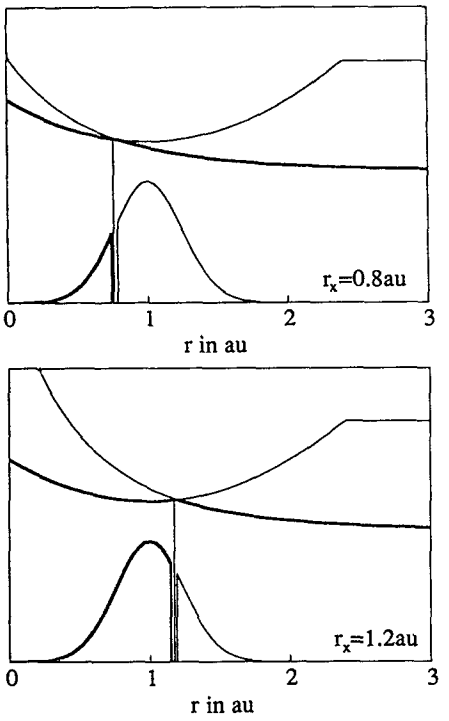

FIG. 10. Schematic view of the diabatic–adiabatic transformation of the wave packets. The upper part of the figures shows the potential energy curves for different r_x. The lower part of the figures shows the splitting of the initial diabatic wave packet: the bold line roughly indicates the part that goes into the lower adiabatic state.

The adiabatic view provides an interpretation of another interesting feature which shows up in the strong coupling case (small b), namely the large shift towards small energy of the main peak in the dissociation energy spectrum (Fig. 11). This shift comes from the existence of two competing "motions": the r motion of the adiabatic wave packet, and the "vertical motion" of the lowest adiabatic energy curve (Fig. 12). Indeed, the dissociation energy depends on these two effects: the particle gains energy when the system dissociates along the lowest adiabatic potential energy curve; however, in the present case, the repulsive potential varies with time (Fig. 12) resulting in a modification of the energy gain. The total energy of the lowest adiabatic wave packet decreases in the first half of the collision when the lowest

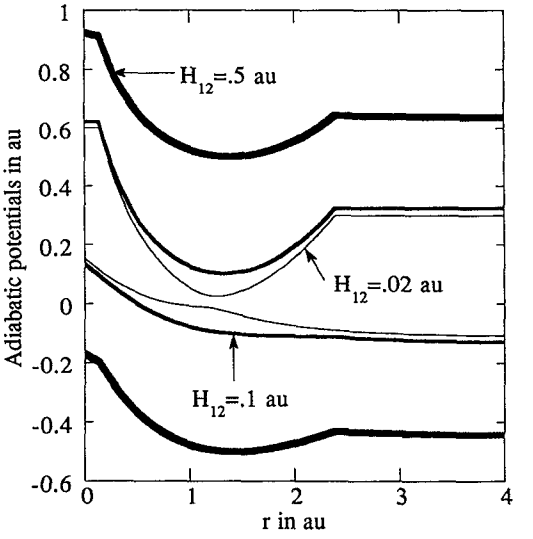

FIG. 12. Adiabatic potential energy curves for a crossing distance $r_x = 1.2$, and for different intermolecular distances R, where the charge exchange interaction is equal to 0.02, 0.1, and 0.5 a.u., respectively.

adiabatic potential energy moves down; on the other hand, it increases in the second half of the collision. If the wave packet has moved away during the collision, the energy decrease is not balanced by the energy increase, then leading to the observed shift of the peak in the dissociation spectrum ("phénomène d'amorti"). Another view can be obtained by looking at the dissociation force $-\partial V/\partial r$ where V is the lowest adiabatic potential. In the strong coupling region, the dissociation force for a given $r > r_x$ is smaller than what it is in the weak coupling region, and can even change sign. As an example, the wave packet can be localized in the well that appears in the lowest adiabatic potential; it must then spend energy to get out of this well. If the vertical motion of the lowest adiabatic curve is too slow (low collision energy), the wave packet can dissociate before the vertical motion occurs, and there is no shift of the dissociation energy peak. Likewise, no shift occurs at higher collision velocity since the adiabatic curve goes up and down before the wave packet can move (Fig. 13).

Such a slowing down of the dissociative wave packet can only be observed if dissociation occurs before the system has reached the turning point. Otherwise, the wave packet cannot experience the variation of the lowest adiabatic energy curve. This explains why the energy spectrum is very different for $r_x > 1$ and $r_x < 1$. In the former case, almost all of the initial wave packet follows the lower adiabatic energy curve, and dissociates before the turning point. On the other hand, if $r_x < 1$, a small part of the initial wave packet dissociates before the turning point, and is slowed down, while the main part of the wave packet which follows the upper adiabatic potential, is preserved against dissociation near the turning point, and partly dissociates in the second half of the collision with roughly the resonance energy (Fig. 14). The appearance of structures in the energy spectrum is attributed to interferences originating from the existence of three different paths for dissociation (Fig. 15): path 1 contributes to the energy spectrum around the resonance energy, and paths 2 and 3 can contribute to smaller energies than the resonance energy.

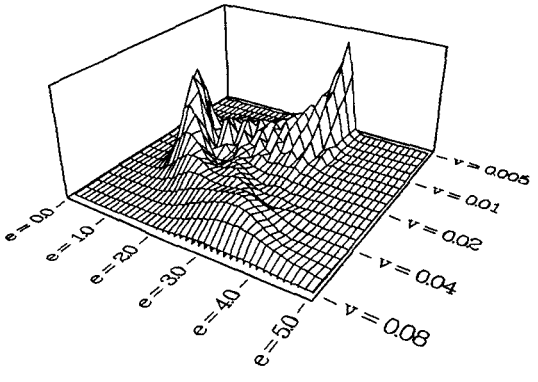

FIG. 13. Velocity dependence of the energy spectrum of the dissociation products in the isotropic case, for $b = 0$ (strong coupling) and $r_x = 1.2$ a.u. The dissociation energy e is in eV, and the collision velocity v is in a.u. The slowing down effect ("amorti") is observed only at intermediate collision velocities.

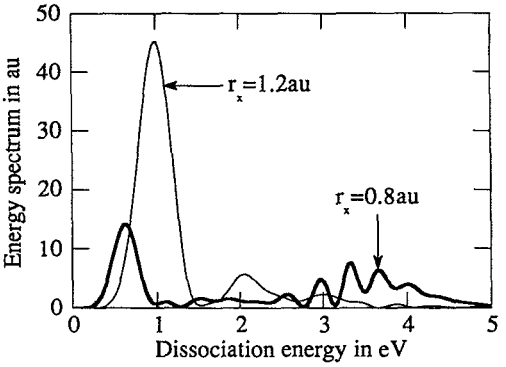

FIG. 14. Energy spectrum of the dissociation products in the isotropic case, for $b = 0$ (strong coupling), $v = 0.02$ a.u. (low collision energy), and different crossing distances ($r_x = 0.8$ and 1.2. a.u.).

C. Anisotropic case

Anisotropic interactions can give rise to a variety of phenomena. Firstly, as in the isotropic case, strong and weak coupling strengths, high or low collision energies must be distinguished, as well as the different relative positions of the diabatic potential curves. Secondly, the change of sign of the considered exchange interaction (Fig. 4) near the turning point can be gradual or sudden (even at low collision energy) depending on the impact parameter b. Only two examples will be presented here, one corresponding to a slowly varying interaction, and the other one to a rapidly varying interaction.

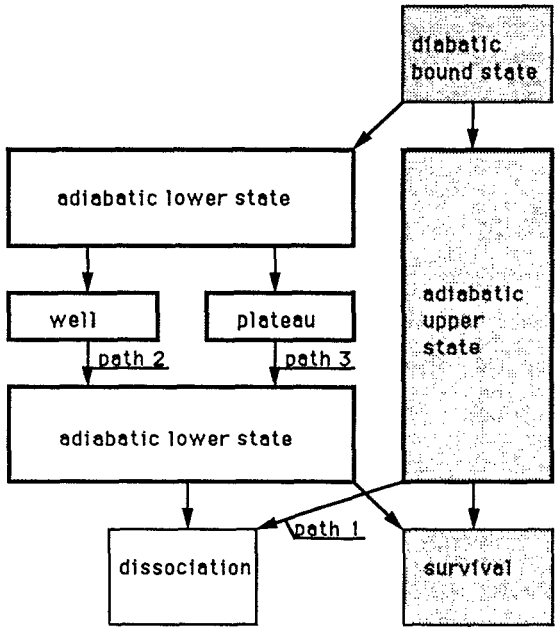

FIG. 15. Chart of the possible paths available to the system in the DCE process for a strong isotropic coupling.

1. Slowly varying interaction

A slow variation of H_{12} occurs when b is large (Fig. 4), and then corresponds to the weak coupling case. Figure 16 shows the dissociative diabatic wave packet for a weak coupling ($b = 3$ a.u.) and a low collision energy. Two different regions of the trajectory, before and after the turning point, contribute to the building up of the dissociative wave packet. If the coupling is low enough, the dissociation probability is small, and the bound wave packet remains essentially unchanged during the whole collision. Thus, the two parts of the dissociative wave packet (emitted respectively in the first and in the second half of the collision) are identical except for the sign (Fig. 16). As a consequence, when the two parts of the dissociating wave packet spread during their propagation, they interfere destructively right at their midpoint: this leads to a dip at the resonance energy in the dissociation spectrum, as already shown in the LCP formalism.[6]

At intermediate impact parameters, the coupling strength becomes large, but it is still slowly varying. The interpretation of the DCE processes in such a situation is the same as in the isotropic case: the initial wave packet can dissociate in the four (instead of two) intermediate coupling regions. In the high coupling region, the wave packets follow the adiabatic energy curves; in the low coupling regions, the diabatic ones. This can give rise to complicated interference effects, since there are quite a few paths (18 different paths) joining the initial diabatic bound state and the final diabatic dissociative state (Fig. 17). As in the isotropic case, only one or all of these paths can be followed during one DCE process, depending on the r_x value.

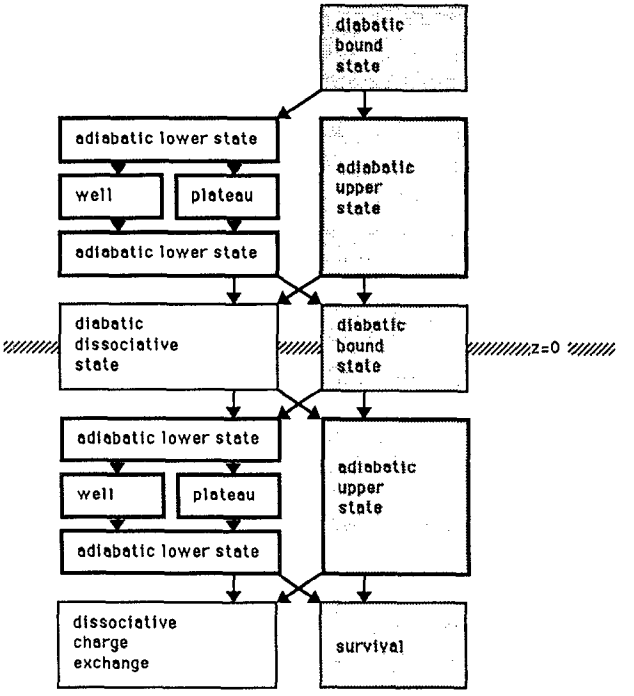

FIG. 17. Chart of the possible paths available to the system in the DCE process for a strong, anisotropic and slowly varying exchange interaction. There are 18 different paths joining the initial state and the final dissociative state.

2. Rapidly varying interaction

New clear-cut phenomena appear due to the sudden variation of $H_{12}(t)$ near the turning point at small impact parameter (Fig. 4). These phenomena show up very clearly for $b = 0$ at low collision energies. Although a straight line trajectory is somewhat unphysical in this case, the situation can be regarded as a model of real trajectory leading to sudden variations of H_{12} (Fig. 18). Indeed, as the R and γ coordinates only appear through $H_{12}[R(t),\gamma(t)]$, no fundamental changes are expected from the existence of a bent trajectory. As already mentioned, our method can apply to any situation involving a time dependent interaction between bound and dissociative molecular states; from this point of view, we are now dealing with phenomena related to a sudden switching of the interaction.

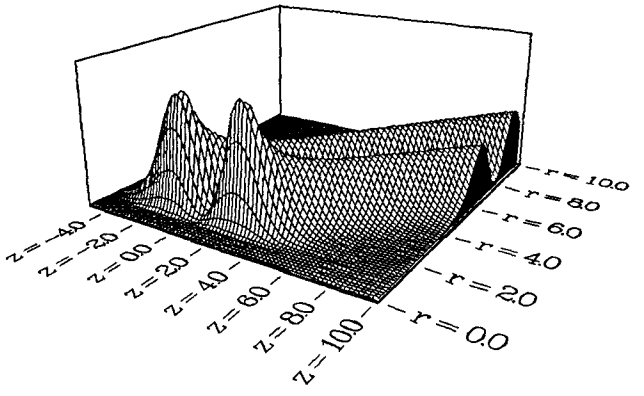

FIG. 16. Time evolution of the probability density associated with the dissociative diabatic state in the anisotropic case ($\theta = 0$), for $b = 3$ a.u. (weak coupling), $v = 0.02$ a.u. (low collision energy), and $r_x = 1.2$ a.u. As the exchange interaction vanishes near the turning point ($z \simeq 0$), the wave packet is emitted before and after the turning point.

As seen in Sec. III B 2, interpretation of the phenomena occurring near the turning point at small b can be done using the adiabatic basis set. It is then more convenient to describe the effects of the H_{12} discontinuity in that basis. The rotation angle α characterizing the diabatic to adiabatic basis change is given by Eq. (30). When $4H_{12}^2 \gg (H_{11} - H_{22})^2$, i.e., near the crossing point of the diabatic energy curves, α increases (or decreases) by $\pi/2$ as a result of the H_{12} jump: the sudden H_{12} jump results in the sudden interchange of the two adiabatic wave packets. In contrast, far from r_x, the change of α as a result of the H_{12} jump is smaller than $\pi/2$ and the sudden interchange of the two adiabatic wave packets is incomplete. The lower adiabatic wave packet may partly escape during the first half of the collision: it is incompletely brought into the upper adiabatic state at $z = 0$. As a result, the part that jumps arrives inside the well and on the dissociation plateau of the upper adiabatic energy curve; this is clearly seen on Fig. 19. On the contrary, as the upper adiabatic wave packet has spent all its life in a well (diabatic, then adiabatic), it is still located near the crossing point at

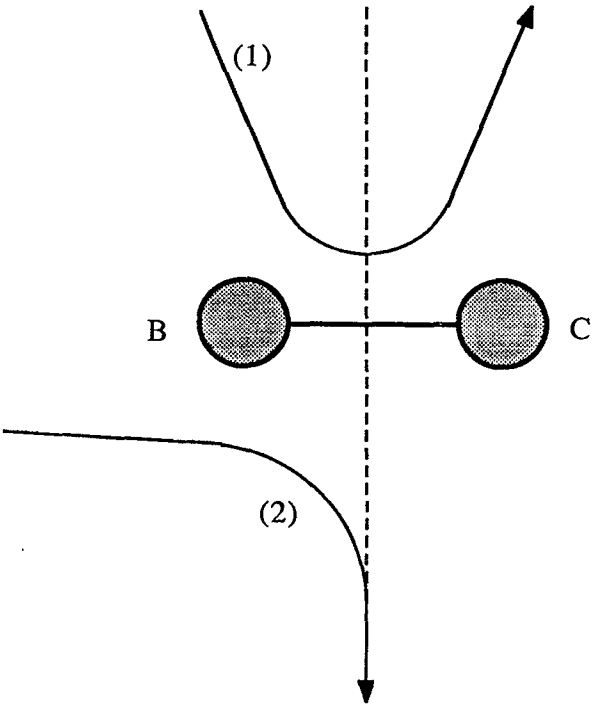

FIG. 18. Examples of bent trajectories leading to a fast variation of the exchange interaction in the anisotropic case. For the trajectory 1, H_{12} is an odd function of time, similar to the straight line trajectory case at $\theta = 0$. In the second trajectory, H_{12} abruptly drops to zero.

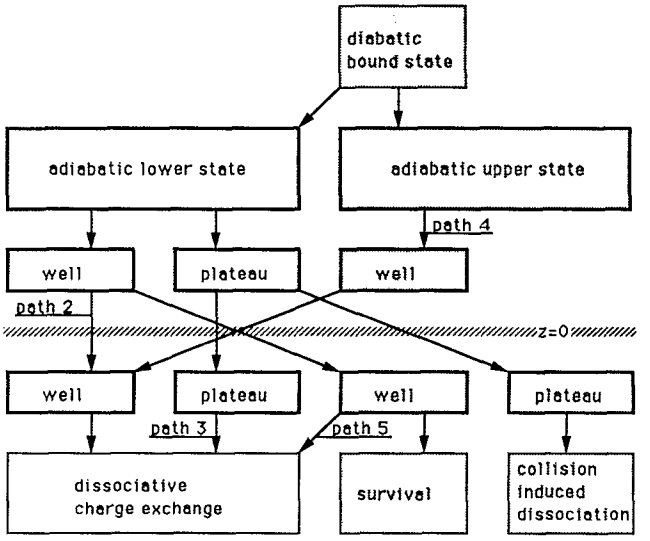

FIG. 20. Chart of the possible paths available to the system in the DCE process for a strong, anisotropic and rapidly varying exchange interaction.

$t = 0^-$. At $t = 0^+$, it is then efficiently brought in the lower adiabatic state.

A schematic diagram of the whole collision process is presented in Fig. 20. Most of the features of the energy spectrum of the dissociation products (Fig. 21) can be understood using this diagram. Paths 2 and 3 were already present in the diagram of Fig. 15, corresponding to the isotropic case. As observed in Sec. III B 2, they give rise to low energy components in the dissociation energy spectrum. The other paths (4 and 5) are specific to the anisotropic case. Path 4 corresponds to the part of the wave packet that was transferred at $t = 0$ from the upper adiabatic well to the lowest adiabatic well; thus it has very little kinetic energy and only contributes to this low energy part of the spectrum. Interference structures in this part of the spectrum arise from the existence of three different paths (2, 3, and 4) leading to low energy products. In path 5, a part of the wave packet begins to escape during the first half of the collision. When H_{12} changes sign, it is moved up to the right side of the upper adiabatic well. It is then trapped in this permanent well with a significant amount of vibrational energy. In the final stage

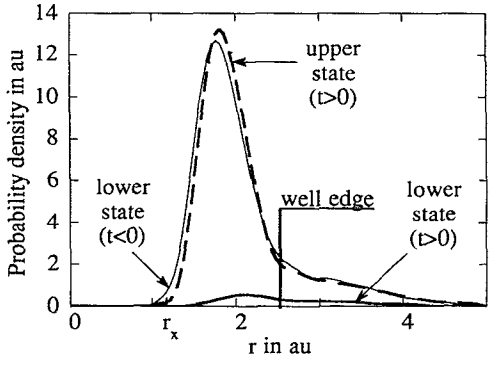

FIG. 19. Probability densities in the adiabatic states near the turning point ($z = 0$), when the exchange interaction is strong and varies abruptly (anisotropic case, $\theta = 0$, $b = 0$, $v = 0.012$ a.u., $r_x = 1.2$ a.u.). Before $z = 0$, the whole wave packet is in the adiabatic lower state. Just after $z = 0$, the main part of the wave packet has jumped into the upper state; a small part can survive in the lower state far from the crossing distance r_x.

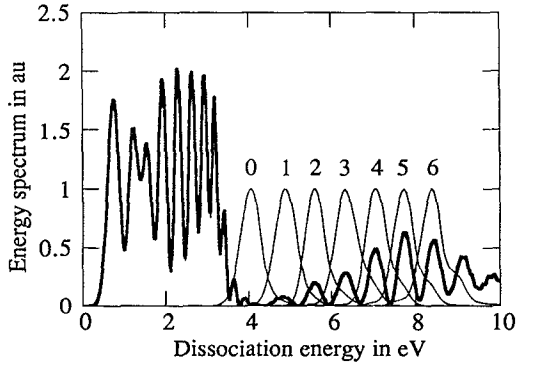

FIG. 21. Energy spectrum of the dissociation products (bold line) obtained in the anisotropic case ($\theta = 0$), for $b = 0$ (strong coupling), $v = 0.012$ a.u. (low collision energy) and $r_x = 1.2$ a.u. The low energy structure is due to the existence of different paths (numbered 2, 3, and 4 in Fig. 20), and the high energy structure shows the onset of the quantization in the adiabatic upper state. This has been proved by launching at $z = 0$ a "half collision" with each of the vibrational eigenstates of the adiabatic upper state. The energy spectra of these half-collisions (thin lines) are numbered according to their initial v states.

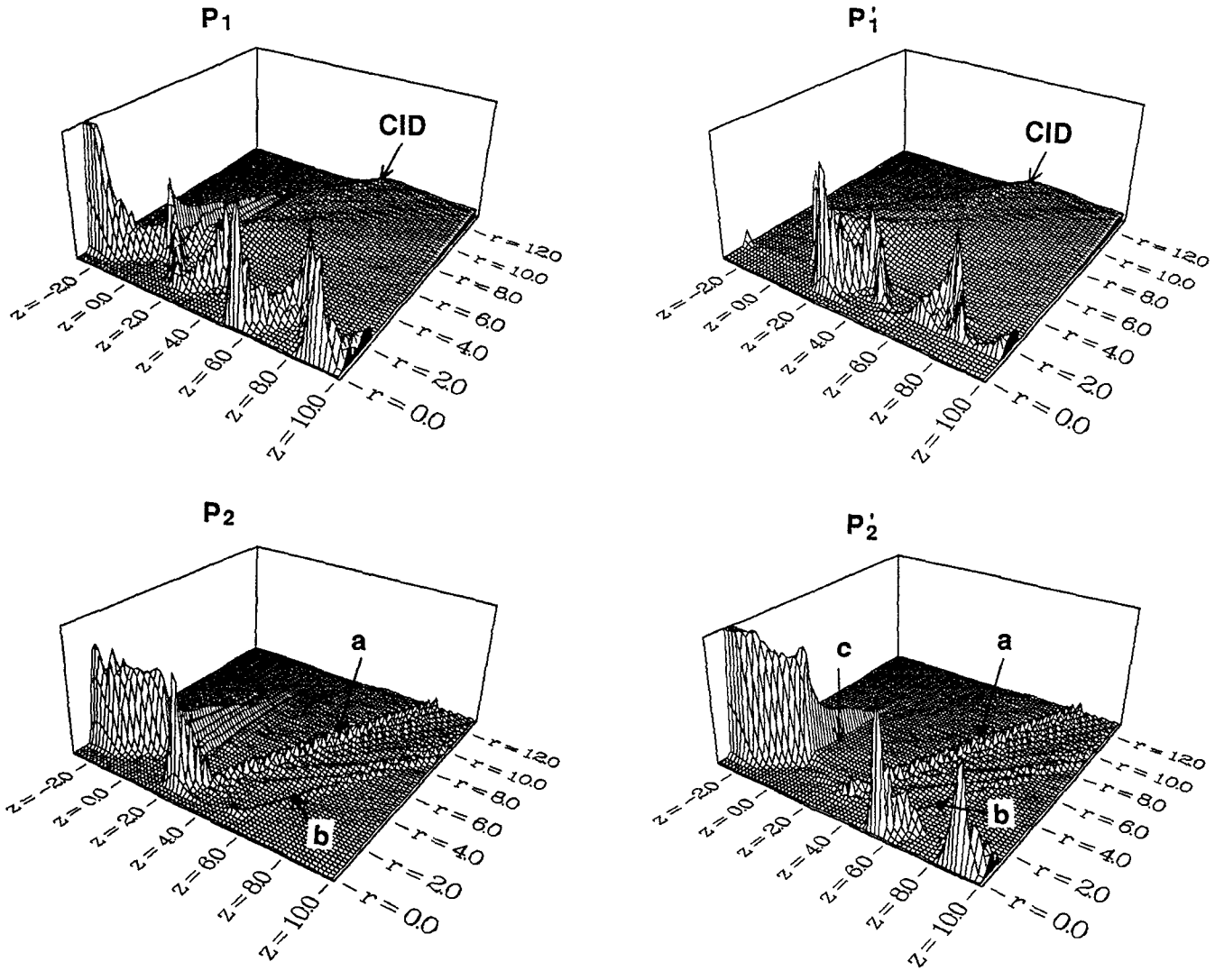

FIG. 22. Probability densities associated with the various wave packets: P_1: diabatic bound, P_2: diabatic dissociative, P_1': upper adiabatic, P_2': lower adiabatic. The collision conditions are the following: anisotropic case, $\theta = 0$, $b = 0$ (strong and rapidly varying exchange interaction), $v = 0.012$ a.u. (low collision energy), $r_x = 1.2$ a.u. During the first half of the collision ($z < 0$), the initial diabatic bound wave packet P_1 goes almost completely into the adiabatic lower state. In this lower state, part of the wave packet escapes before $z = 0$, while the other part is trapped in the well appearing at strong H_{12}. At $z = 0$, the sudden change of sign of H_{12} brings the main part of the wave packet P_2' from the lower to the upper adiabatic state. The vibration of the molecule starting at $z = 0$ is clearly seen on the P_1' wave packet in the strong coupling region ($z < 4$ a.u.), and on the P_1 wave packet at large z. Similarly, collision induced dissociation (CID) appears in P_1' after $z = 0$ as a wave moving to large r. In the intermediate coupling region, during the molecule vibration, two transitions occur toward the dissociation channel; they give rise to the two wavelets (a and b), rapidly moving out to large r. The ripples seen between a and b result from the interference of the a and b waves with the small part c of the P_2' wave packet which remains in the lower adiabatic state after the H_{12} jump at $t = 0$.

of the collision, when H_{12} decreases, part of this adiabatic wave packet feeds the diabatic dissociative wave packet: this energetic wave packet contributes to the high energy part of the dissociation spectrum above the resonance energy. During this final stage, the upper adiabatic wave packet performs about two oscillations in its well; at each passage near r_x, part of this wave packet is transferred into the dissociation channel. These two contributions interfere, leading to the structures in the high energy region of Fig. 21. Therefore, this structure represents the vibrational structure of the time dependent adiabatic upper state. This explanation has been verified by studying a "half-collision" process starting at $t = 0$ with a wave packet corresponding to a given vibrational eigenstate of the upper adiabatic state. At the end of the half-collision process, each vibrational state gives rise to a peak; all these peaks match the interference structure discussed above.

All the phenomena, put forward in the analysis of the dissociation spectrum, can indeed be visualized on Fig. 22 which presents the time dependence of both the adiabatic and diabatic wave packets.

IV. CONCLUSION

In the present paper, we have reported on a new coupled wave packet method that allows the treatment of nonadiaba-

tic vibronic processes. It is designed to describe quantally dissociative processes and provides an exact solution within the semiclassical approximation.

As an illustrative example, the method has been applied to prototype dissociative charge exchange processes. These prototypes reveal a number of general features that are expected to appear in real systems. For example, the dissociation energy spectra of DCE processes exhibit very low and high energy components, as well as interference structures. By scrutinizing the time evolution of the wave packets, it has been possible to understand these features in terms of the competition between two motions of the wave packets in the diabatic basis set:

-the bound and dissociative wave packets evolve along their own electronic energy curve (r motion);

-the wave packets oscillate between the two electronic diabatic states, due to the electronic coupling.

The analysis of the wave packets in the adiabatic basis set can also be used to get insight into the dynamics of the problem. Indeed, in the strong coupling regions, the adiabatic wave packets are almost decoupled and evolve along the adiabatic energy curves. In the intermediate coupling region, the study of the time evolution of the diabatic and/or adiabatic wave packets allows the analysis of the passage between the adiabatic and diabatic behaviors. In addition, we have shown that new effects show up when the charge exchange interaction undergoes a rapid variation. These effects result from sudden transitions in the adiabatic basis; they appear in the case of anisotropic charge exchange interactions at small impact parameters.

In conclusion, the coupled wave packet method is an efficient means of treating the general dissociative processes in atom–molecule collisions (e.g., DCE, CID). Its very broad applicability enables to uncover new effects that could not be reached by the previously available approximate methods. Besides, the display of the time dependence of the wave packets provides a direct view of the quantal collision dynamics which sometimes retrieves underlying classical motions.

[1] R. Johnsen and M. A. Biondi, J. Chem. Phys. **61**, 2112 (1974).
[2] D. P. de Bruijn, J. Neuteboom, V. Sidis, and J. Los, Chem. Phys. **85**, 215 (1984).
[3] V. Sidis, J. Phys. Chem. **93**, 8128 (1989).
[4] V. Sidis and D. P. de Bruijn, Chem. Phys. **85**, 201 (1984).
[5] Y. N. Demkov, Sov. Phys. JETP **18**, 138 (1964); E. E. Nikitin, in *Advances in Quantum Chemistry* (Academic, New York, 1970), Vol. 5, p. 135.
[6] V. Sidis and C. Courbin-Gaussorgues, Chem. Phys. **111**, 285 (1987).
[7] J. P. Gauyacq, J. Phys. B **13**, 4417, L-501 (1980); *Dynamics of Negative Ions* (World Scientific, Singapore, 1987).
[8] C. Bottcher, in *Electronic and Atomic Collisions*, edited by J. Eichler, I. V. Hertel, and N. Stolterfoht (Elsevier, Houston, 1984), p. 187.
[9] J. Alvarellos and H. Metiu, J. Chem. Phys. **88**, 4957 (1988).
[10] A. E. Orel and K. C. Kulander, Chem. Phys. Lett. **146**, 428 (1988).
[11] J. P. Gauyacq and V. Sidis, Europhys. Lett. **10**, 225 (1989).
[12] F. T. Smith, Phys. Rev. **179**, 111 (1969); C. Kubach and V. Sidis, Phys. Rev. A **14**, 153 (1976); J. C. Tully, in *Dynamics of Molecular Collisions*, W. H. Miller (Plenum, New York, 1976), p. 217; V. Sidis, in *Collision Theory for Atoms and Molecules*, edited by F. A. Gianturco, NATA-ASI series (Plenum, New York, 1989).
[13] M. A. Wartell and R. J. Cross, J. Chem. Phys. **55**, 4983 (1971).
[14] B. M. Smirnov, *Asymptotic Methods in the Theory of Atomic Collisions* (Atomizdat, Moscow, 1973); V. I. Bilkin, L. A. Pakina, and B. M. Smirnov, Sov. Phys. JETP **32**, 540 (1971); A. V. Evseev, A. A. Radstig, and B. M. Smirnov, *ibid.* **50**, 283 (1980); J. Phys. B **15**, 4437 (1982).
[15] R. Kosloff, J. Phys. Chem. **92**, 2087 (1988).
[16] W. H. Press, B. P. Flannery, S. A. Teukolsky, and W. T. Vetterling, *Numerical Recipes* (Cambridge University, Cambridge, 1987), p. 636.